

Are there radio-loud and radio-quiet Gamma-Ray Bursts?

Joshua A. Osborne^{1*} Fatemeh Bagheri^{1†} Amir Shahmoradi^{1,2‡}

¹*Department of Physics, College of Science, The University of Texas, Arlington, TX 76010, USA*

²*Data Science Program, College of Science, The University of Texas, Arlington, TX 76010, USA*

20 October 2020

ABSTRACT

The potential existence of two separate classes of Long-duration Gamma-Ray Bursts (LGRBs) with and without radio afterglow emission, corresponding to radio-bright/loud and radio-dark/quiet populations, has been recently argued and favored in the GRB literature. The radio-quiet LGRBs have been found to have, on average, lower total isotropic gamma-ray emissions (E_{iso}) and shorter intrinsic prompt gamma-ray durations (e.g., T_{90z}). In addition, a redshift $-T_{90z}$ anti-correlation has been discovered among the radio-loud LGRBs, which is reportedly missing in the radio-quiet class. Here we discuss the significance of the differences between the energetics and temporal properties of the two proposed classes of radio-loud and radio-quiet LGRBs. We show that much of the proposed evidence in support of the two distinct radio populations of LGRBs can be explained away in terms of selection effects and sample incompleteness. Our arguments are based on the recent discovery of the relatively-strong highly-significant positive correlation between the total isotropic emission (E_{iso}) and the intrinsic prompt duration (T_{90z}) that is present in both populations of short-hard and long-soft GRBs, predicted, quantified, and reported for the first time by Shahmoradi (2013) and Shahmoradi & Nemiroff (2015).

Key words: methods: analytical – methods: numerical – methods: statistical – gamma-ray burst: general

1 INTRODUCTION

Gamma-ray bursts (GRBs) are extremely energetic explosions, the long-duration class of which has been long hypothesized to be due to the death super-massive stars, releasing energies on the orders of 10^{48} to 10^{52} ergs (e.g., Frail et al. 2001; Cenko et al. 2010; Shahmoradi & Nemiroff 2015) and occur at distances far from us on the cosmological scale (Metzger et al. 1997). The current afterglow model is that of an expanding fireball (Piran 1999; Meszaros 2002; Woosley & Bloom 2006) where the high energy prompt gamma-ray emission is first observed, followed by afterglow emission at lower-energy frequencies after a few hours or days from the initial gamma-ray prompt emission (Frail et al. 1997; Van Paradijs et al. 1997; Heng et al. 2008).

The standard fireball model used today was proposed after the first observation of both X-ray and optical afterglows in February of 1997 (Kumar & Zhang 2015). Not long after, the first GRB *without* an optical afterglow

counterpart was found (Groot et al. 1998). This class of bursts without optical afterglows became known as the *dark GRBs* (Fynbo et al. 2001). On October 9, 2000, however, the second High Energy Transient Explorer (HETE-2) (Ricker et al. 2003) was launched and in December of 2002 it viewed it's first dark GRB where the optical afterglow was seen, but disappeared and was no longer visible after 2 hours. This begged the question, is there ever truly such a phenomenon as a *dark GRB* or is it possible that with better equipment and timing no such phenomena would ever appear?

More recently, studies have raised the possibility of the existence of a new population of Long-duration GRBs (LGRBs) that are intrinsically dark in the radio-bandwidth afterglow. These events, named ‘radio-dark’, ‘radio-quiet’, or ‘radio-faint’ LGRBs, have been hypothesized to have progenitors that are different from the progenitors of the mainstream ‘radio-bright’ or synonymously-named ‘radio-loud’ LGRBs (e.g., Hancock et al. 2013; Lloyd-Ronning & Fryer 2017; Lloyd-Ronning et al. 2019).

Alternative hypotheses on the lack of detection of radio afterglows in some LGRBs have been also studied

* E-mail: joshua.osborne@uta.edu (JAO)

† E-mail: fatemeh.bagheri@uta.edu (FB)

‡ E-mail: a.shahmoradi@uta.edu (AS) (corresponding author)

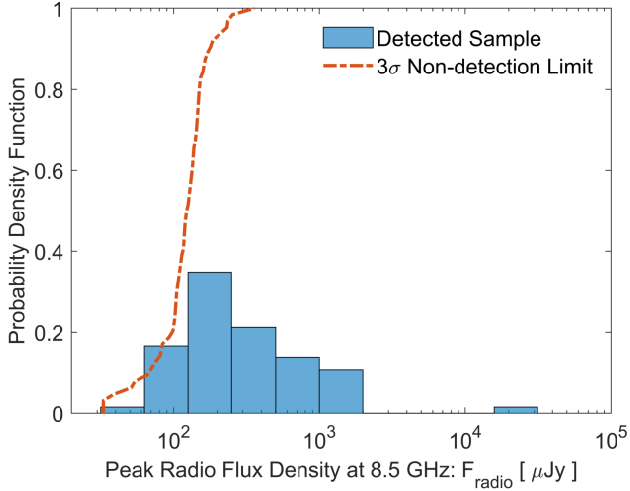


Figure 1. Histogram of the normalized count (probability density function) of 66 radio-loud GRBs taken from [Chandra & Frail \(2012\)](#). The dashed-dotted red line represents the Cumulative Probability Density Function of the 3σ upper-limits for the non-detection of radio afterglows of 107 radio-quiet GRBs.

(e.g., [Frail 2005](#); [Chandra & Frail 2012](#)). In particular, [Chandra & Frail \(2012\)](#) used a comprehensive sample of 304 afterglows, consisting of 2995 flux density measurements at a wide range of frequencies between 0.6 GHz and 660 GHz, to argue against the potential existence of radio-bright and radio-dark LGRBs. The argument therein is based on the observation that the 3σ upper-limit for the non-detection of the radio afterglow of radio-dark LGRBs closely traces the faint-tail of the radio-bright LGRB sample, as illustrated in Figure 1.

Responding to these observations, [Hancock et al. \(2013\)](#) employed image stacking techniques to increase the overall signal in the combined data from all radio-quiet GRBs. Based on their own specific classification, they conclude that radio-dark LGRBs are on average 2-3 orders of magnitude fainter than radio-bright LGRBs. Such result is not surprising and is in fact, relatively consistent with the observational sample of [Chandra & Frail \(2012\)](#), illustrated in Figure 1.

Nevertheless, based on simulations of the radio afterglows of LGRBs, [Hancock et al. \(2013\)](#) predict that the expected stacked radio flux density of radio-dark LGRBs must be on average 5 times brighter in order to be consistent with the hypothesis of a common continuous unimodal distribution for the radio afterglow properties of all LGRBs together. However, they acknowledge several limitations of their simulations, most importantly, the assumption that the observed sample of radio-afterglows in their studies is representative of the radio afterglow properties of the entire underlying population of detected and undetected LGRBs.

Most recently, [Lloyd-Ronning et al. \(2019\)](#) (hereafter [L19](#)) build upon the existing sample of the GRB radio afterglows of [Chandra & Frail \(2012\)](#) to further confirm and strengthen the findings of their previously published study ([Lloyd-Ronning & Fryer 2017](#)) on the fundamental spec-

tral and temporal differences and similarities of the radio-quiet and radio-loud GRBs in multiple observational bandwidths including optical, x-ray, gamma-ray and GeV emission. Specifically, they find that,

(i) The total isotropic gamma-ray emission (E_{iso}) does not correlate with the radio luminosity in their observational samples of 78 radio-loud and 41 radio-quiet LGRBs.

(ii) Radio-quiet LGRBs have significantly lower total isotropic gamma-ray emission (E_{iso}), on average, 5 times lower than the radio-loud LGRBs.

(iii) Radio-quiet LGRBs have significantly shorter intrinsic prompt duration as measured by the quantity T_{90z} (see for example, [Shahmoradi 2013c](#); [Shahmoradi & Nemiroff 2015](#)), than the radio-loud LGRBs.

(iv) Radio-quiet LGRBs exhibit a weak positive $E_{\text{iso}} - T_{90z}$ correlation whereas this correlation is missing in the radio-loud LGRBs.

(v) Radio-quiet LGRBs exhibit a weak negative correlation between T_{90z} and redshift (z) whereas the radio-loud LGRBs exhibit a much stronger such correlation.

(vi) The very high energy (0.1 – 100 GeV) extended emission is only present in the radio-loud sample.

(vii) Also, there is no significant difference in the the redshift distribution, the presence of X-ray/optical plateaus, or the average jet opening angles between the two radio-quiet and radio-loud GRB samples.

Such observational evidence in favor of the two classes of radio-loud and radio-quiet LGRBs can have profound implications for the progenitors of LGRBs as highlighted and discussed by [L19](#). However, here we argue and show that much of the above evidence in favor of the two fundamentally-distinct radio-quiet and radio-loud GRBs can be potentially explained in terms of the existing correlation between E_{iso} and T_{90z} of both long and short duration classes of GRBs. To the extent of our knowledge, this positive $E_{\text{iso}} - T_{90z}$ correlation in both classes of LGRBs and short-duration GRBs (SGRBs) was originally discovered, quantified, and reported for the first time by [Shahmoradi \(2013c\)](#) and [Shahmoradi & Nemiroff \(2015\)](#) via a careful analysis of the largest catalog of GRBs available at the time. Hints to the existence of such a correlation has been also independently provided by [Butler et al. \(2010\)](#). The relationship has been also rediscovered recently in an independent study of a sample of Swift-detected GRBs ([Tu & Wang 2018](#)).

In the following sections, we consider the arguments in favor of the existence of two separate populations of radio-loud and radio-quiet GRBs and show that much of the evidence provided can be likely explained in terms of strong selection effects and sample incompleteness of the radio afterglow data and the existing correlations among the spectral and temporal properties of LGRBs as discovered and quantified by [Shahmoradi \(2013c\)](#); [Shahmoradi & Nemiroff \(2015\)](#).

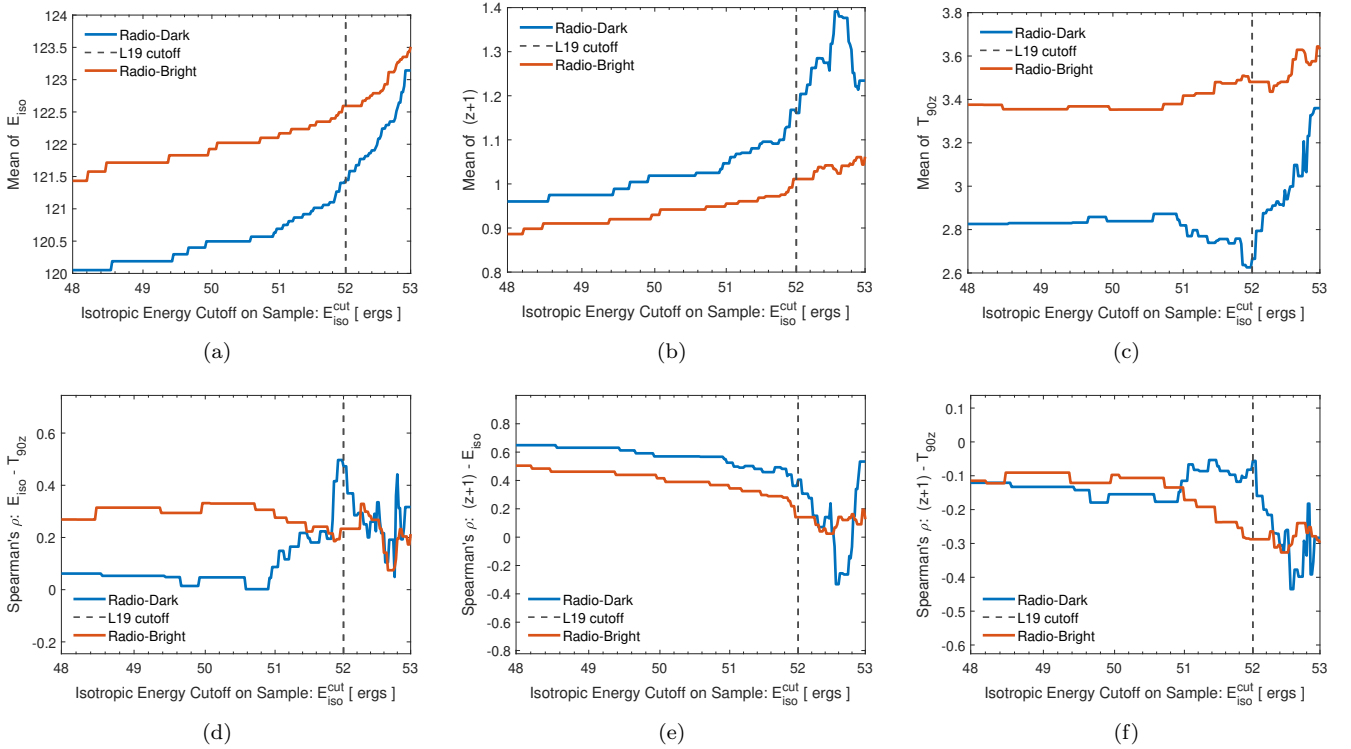


Figure 2. A depiction of the dynamics of different properties of the radio-loud and radio-quiet LGRBs as a function of the sample selection cutoff. The dashed line represent the cutoff used in the study of L19 to generate a sample of bright LGRBs. As evidenced, some of the differing attributes of the two classes appear to be highly sensitive to the arbitrarily chosen sample selection cutoff value used in L19, most importantly, the correlations between redshift (z), isotropic emission (E_{iso}), and intrinsic duration (T_{90z}).

2 AN ALTERNATIVE INTERPRETATION FOR THE EXISTENCE OF RADIO LOUD AND QUIET LGRBS

To better quantify the differences between the two hypothesized radio classes, we first apply the statistical bootstrapping (e.g., Efron & Tibshirani 1994) technique to the radio-loud and radio-quiet samples of L19 to form confidence bounds on the mean and standard deviations of the two populations, as well as the correlation strengths between the three quantities: redshift (z), the total isotropic gamma-ray emission (E_{iso}), and the intrinsic duration (T_{90z}). In brief, bootstrapping is a statistical resampling method (with replacements) that, in the absence of multiple independent sets of observational data, can provide confidence bounds on the various statistical properties of a dataset.

In the following sections, we discuss and quantify the significance of each of the differences and similarities of the two radio-loud and radio-quiet LGRBs as quantified by the bootstrap confidence bounds and provide further evidence from Monte Carlo simulations that shed light on the classification of the radio emissions of LGRBs.

2.1 The redshift distributions of radio-loud and radio-quiet LGRBs

Figure 3 displays the bootstrapping results for some of the statistical properties of the two radio classes of

L19. The first and foremost quantity in the studies of cosmological objects is redshift (z). Similar to L19, we find the redshift distributions of the two classes of radio-loud and radio-quiet LGRBs are consistent with hypothesis of belonging to the same parent population distribution. A two-sample Kolmogorov-Smirnov test on the two redshift distributions reveals no significant difference between the two redshift distributions, that is, we cannot reject the null hypothesis that the two redshift samples originate from the same distribution with a KS-test probability of $\rho \sim 0.24$.

We note, however, that this hypothetical parent distribution for the redshifts of the two classes is likely severely affected by selection effects due to the gamma-ray detection and the redshift measurement thresholds. We find the average redshifts of the radio-quiet and radio-loud samples to be $\bar{z}_{\text{loud}} \sim 2.21 < \bar{z}_{\text{quiet}} \sim 2.6$. This is contrary to the reported value for \bar{z}_{loud} in Table (1) of L19. Nevertheless, our bootstrapping simulations indicate that the differences in the redshift averages are insignificant as illustrated in Figure 3a. There is a 0.14 probability that the average redshift of the radio-loud sample could be actually larger than the average redshift of the radio-quiet sample. The dispersion in the redshift distributions of the two radio classes also appear to be consistent with each other as depicted by the bootstrapping results in Figure 3d.

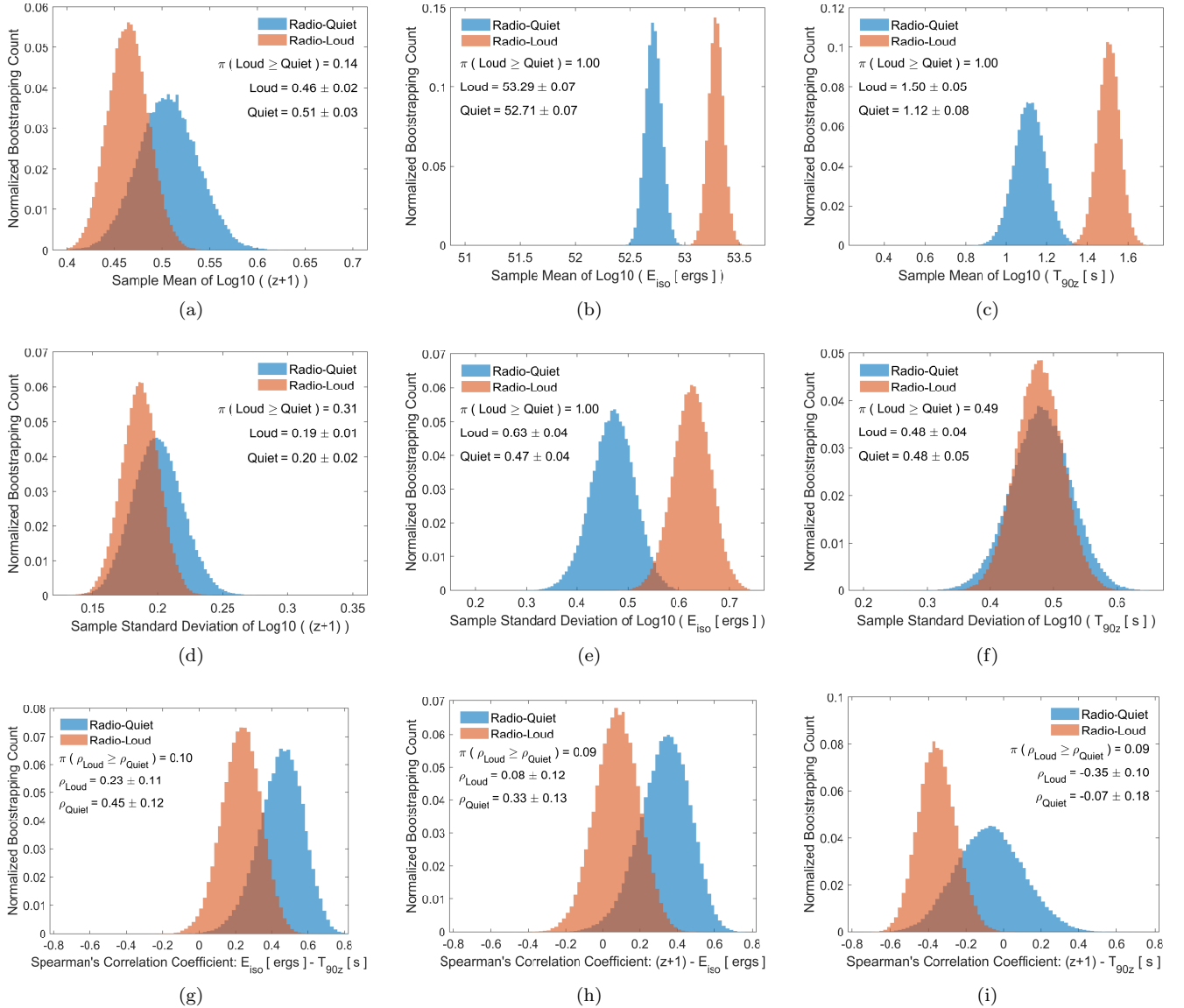


Figure 3. The bootstrapping simulation results for the some of the population properties of the two classes of radio-loud and radio-quiet LGRBs. Plots (a), (b), (c) display respectively, the bootstrapping distributions of the averages of the distributions of $z + 1$, E_{iso} , T_{90z} distributions of the two radio classes. In the same order, plots (d), (e), (f) display the corresponding bootstrapping distributions of the standard deviations of the three LGRB property distributions for the two classes. Plots (g), (h), (i) display the bootstrapping distributions of the Spearman's correlation strengths between the three LGRB properties. The inset values represent the mean and the 1σ dispersions in the bootstrap distributions in each plot, with $\pi(\cdot)$ denoting the probability and ρ denoting the Spearman's correlation strength.

2.2 The energetics of radio-loud and radio-quiet LGRBs

Similar to L19, the results of our bootstrapping simulations indicate a strong evidence, at almost 100% confidence level, that the average and the standard deviation of the E_{iso} distribution of the radio-loud LGRBs are larger than the average and the standard deviation of the E_{iso} distribution of the radio-quiet sample (Figures 3b & 3e). However, unlike L19, here we hypothesize a different origin for the observed differences in the E_{iso} distributions of the radio-loud and radio-quiet LGRBs.

Our *fundamental hypothesis* in this work is that *there is potentially a significant (but not necessarily strong) positive correlation between the radio-afterglow and the prompt gamma-ray energetics of LGRBs*. Such a hypothesis may not be too far from reality as there has been already evidence for the potential existence of a positive correlation between the total isotropic gamma-ray emission (E_{iso}) of GRBs with their peak radio luminosity at 8.5 GHz (L_{rad}). In Figure 4a, we have regenerated the plot of Figure 20 in Chandra & Frail (2012). We find a positive Spearman's correlation strength of $\rho \sim 0.45$ for the $E_{\text{iso}} - L_{\text{rad}}$ relationship.

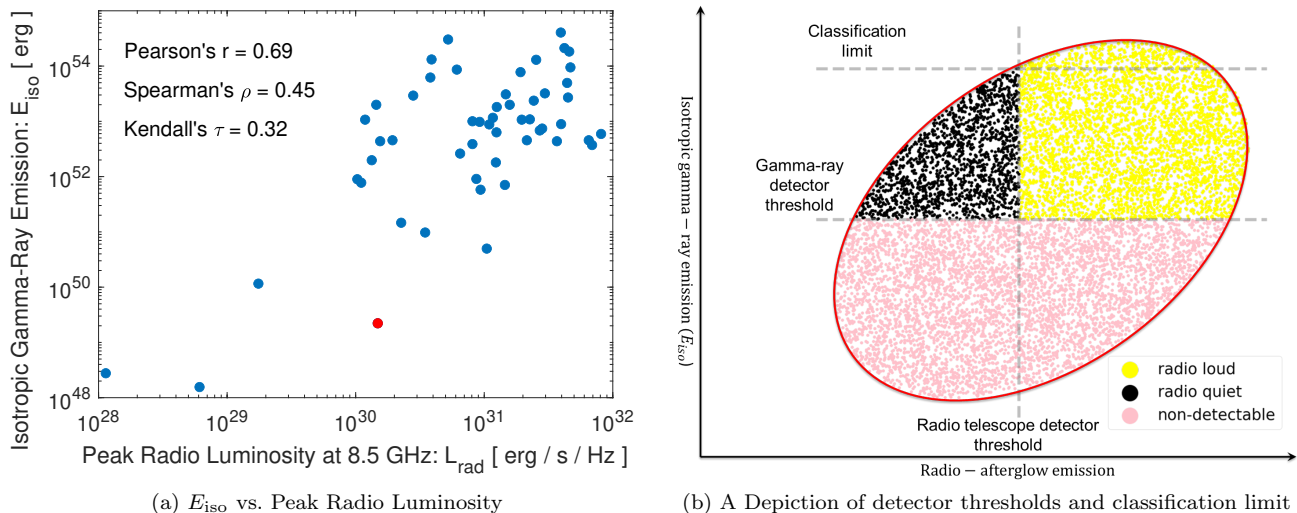


Figure 4. (a): An illustration of the observational sample of Chandra & Frail (2012) showing the relationship between E_{iso} and the peak radio luminosity. The only X-Ray Flash (XRF) event in the sample of Chandra & Frail (2012) is shown by the red point. Exclusion of the XRF from the plots results in a minor decrease in the Spearman’s correlation strength from $\rho = 0.45 \pm 0.13$ to $\rho = 0.43 \pm 0.13$. (b): A schematic illustration of the combined effects of the gamma-ray and radio detection thresholds as well as the potential existence of an underlying correlation between the radio and gamma-ray emissions of LGRBs on the observed LGRBs sample and how these factors can lead to the appearance of two separate classes of radio-loud and radio-quiet LGRBs. The red oval represents the positive underlying correlation between E_{iso} and the radio emission. However, the gamma-ray detector threshold (and the complex redshift selection effects) impose a severe cut on the y-axis, hiding much of the cosmic population of LGRBs (represented by the pink color) from our view. Simultaneously, the radio detector threshold effects, place another severe cut on the observed sample of LGRBs to create an impression of two separate classes of radio-loud and radio-quiet LGRBs. Because of the positive correlation of E_{iso} with the radio emission, any LGRB above a certain E_{iso} threshold (i.e., the *radio classification limit*) will be automatically *always* classified as a radio-loud event. This leads to an apparent increase in the average E_{iso} of the radio-loud sample (represented by the yellow-colored points) relative to the radio-quiet sampled (represented by the black-colored points), similar to what has been reported in the literature as the differing characteristics of radio-quiet and radio-loud LGRBs.

The scatter in the underlying intrinsic $E_{\text{iso}} - L_{\text{rad}}$ correlation of the LGRBs population is likely different from what is seen in Figure 4a since the distributions of both quantities E_{iso} and L_{rad} are severely affected by the corresponding gamma-ray and radio detector thresholds. We defer a quantification of this relationship to a future work and suffice, in this work, to only note the high plausibility of the validity such hypothesis given the existing evidence. Hints to the existence of correlations between the prompt gamma-ray and afterglow emissions in wavelengths other than radio have been also provided by other independent studies (e.g., Margutti et al. 2013; Dainotti & Del Vecchio 2017).

The existence of such correlation between the radio and gamma-ray energy releases would readily explain the appearance of the two classes of radio-quiet and radio-loud LGRBs: **The more energetic LGRBs in gamma-ray emission tend to be more luminous in radio afterglows, and therefore, tend to be classified as radio-loud LGRBs more frequently.** Consequently, radio-loud LGRBs appear to be much more energetic as measured by E_{iso} relative to radio-quiet LGRBs. This phenomenon is well illustrated in the schematic plot of Figure 4b where the effects of the radio and gamma-ray detector thresholds create apparently two distinct classes of radio loud and quiet LGRBs with significantly different characteristics, similar in behavior to the findings of L19.

As illustrated in Figure 4b, when LGRBs reach a certain gamma-ray emission as measured by E_{iso} , their radio-emission also surpasses the radio-emission detection threshold. Therefore, LGRBs beyond a certain E_{iso} threshold are automatically classified as radio-loud LGRBs. This results in the apparent segregation of the LGRB population into two distinct groups whose E_{iso} distributions are different despite having the same redshift distributions. Indeed, L19 report such excess in the average energetics of their radio-loud LGRB sample relative to radio-quiet LGRBs (e.g., see the middle plots of Figures 1 & 2 of L19 and Figure 3b in this work). Meanwhile, the presence of two strong and independent radio and gamma-ray detection thresholds on the bivariate $E_{\text{iso}} - T_{90z}$ distribution severely undercuts any traces of a significant $E_{\text{iso}} - E_{\text{rad}}$ correlation, where E_{rad} denotes the total radio emission.

The above alternative hypothesis for the origins of the two radio classes automatically provides also a natural explanation for the significantly smaller dispersion in the E_{iso} distribution of radio-quiet LGRBs relative to the radio loud sample, which is evident the middle plots of Figures 1 & 2 of L19 and Figure 3e in this work. The E_{iso} distribution of the radio-quiet sample is strongly affected by the gamma-ray detection threshold and redshift-measurement selection effects in its lower tail and, by the radio-loud classification limit at its upper tail. However, in the case of radio-loud LGRBs, such radio-classification upper limit on the E_{iso} distribution

does not exist and the lower-limit on this distribution is also vaguely defined by a classification limit whose sharpness depends on the strength of the $E_{\text{iso}} - E_{\text{rad}}$ correlation. These effects are well-illustrated in Figure 4b.

2.3 The duration distribution of radio-loud and radio-quiet LGRBs

As soon as the origins of the energetics differences between the radio-loud and radio-quiet LGRBs are understood and accepted as explained in the previous section, the apparent differences between the duration distributions of radio-loud and radio-quiet LGRBs can be also readily explained. We do so by utilizing the recent discovery of the potential existence of a strong positive correlation between the gamma-ray energetics of LGRBs and their intrinsic durations, $E_{\text{iso}} - T_{90z}$, quantified for the first time in a series of works by Shahmoradi (2013c,a); Shahmoradi & Nemiroff (2015, 2019a); Shahmoradi & Nemiroff (2019b); Osborne et al. (2020a); Osborne et al. (2020b).

Plot (b) of Figure 5 displays a reproduction of the LGRB world model of Shahmoradi & Nemiroff (2019a); Osborne et al. (2020a) who find an underlying Pearson's correlation coefficient of $\rho \sim 0.5 - 0.6$ between the intrinsic cosmic distributions of E_{iso} and T_{90z} in log-log space. Interestingly, Shahmoradi & Nemiroff (2015) discover a correlation of similar strength and significance to that of LGRBs in the population of SGRBs.

Since the radio-loud sample of LGRBs has, on average, higher E_{iso} than the radio-quiet LGRBs (by about 0.58 dex as illustrated in Figure 3b, the strong positive $E_{\text{iso}} - T_{90z}$ correlation depicted in plot (b) of Figure 5 also necessitates, on average, higher T_{90z} values for radio-loud LGRBs relative to the radio-quiet sample. Such difference has been indeed reported by L19 (e.g., see the middle plots of Figures 1 & 2 of L19 and Figure 3c in this work).

This resolves the source of another apparent major difference between the two radio classes. In the following sections, we present the results from the Monte Carlo simulations of an LGRB world model in which we attempt to synthetically reconstruct the gamma-ray emission properties of the radio-loud and radio-quiet samples of L19. We show that the population-property differences between the two classes as enumerated in §1 naturally emerge from the combined effects of the gamma-ray detection threshold, the artificial cuts on the observational data, and the intrinsic correlations between the prompt gamma-ray properties of LGRBs as reported by Shahmoradi (2013c); Shahmoradi & Nemiroff (2015).

3 THE LGRB WORLD MODEL

In a series of works, Shahmoradi (2013c); Shahmoradi (2013b); Shahmoradi & Nemiroff (2015, 2019a); Shahmoradi & Nemiroff (2019b); Osborne et al. (2020a); Osborne et al. (2020b) have presented evidence for the existence of a significant positive $E_{\text{iso}} - T_{90z}$ correlation of strength $\rho \sim 0.5 - 0.6$ in both populations LGRBs and

Table 1. Pearson's correlation coefficients of the prompt gamma-ray emission properties of LGRBs inferred from the LGRBs cosmic rate estimates of Shahmoradi & Nemiroff (2019a); Osborne et al. (2020a), assuming the LGRB rate density models of Hopkins & Beacom (2006) and B10.

Parameter	H06	B10
Redshift Parameters		
z_0	0.97	0.97
z_1	4.5	4.00
γ_0	3.4	3.14
γ_1	-0.3	1.36
γ_2	-7.8	-2.92
Correlation Coefficients		
$\rho_{L_{\text{iso}}-E_{\text{pz}}}$	0.53 ± 0.07	0.60 ± 0.05
$\rho_{L_{\text{iso}}-E_{\text{iso}}}$	0.93 ± 0.01	0.95 ± 0.01
$\rho_{L_{\text{iso}}-T_{90z}}$	0.39 ± 0.09	0.37 ± 0.07
$\rho_{E_{\text{pz}}-E_{\text{iso}}}$	0.62 ± 0.05	0.69 ± 0.03
$\rho_{E_{\text{pz}}-T_{90z}}$	0.29 ± 0.04	0.34 ± 0.05
$\rho_{E_{\text{iso}}-T_{90z}}$	0.54 ± 0.05	0.50 ± 0.05

SGRBs. Here, we build upon these works to create a Monte Carlo universe of LGRBs which are subjected to the detection thresholds of BATSE and Swift Burst-Alert-Telescope (BAT) detector thresholds. Since the majority of the events in the radio-loud and radio-quiet LGRB samples of L19 belong to the Swift catalog, here we only present the results for the case of the Swift BAT.

Shahmoradi (2013c); Shahmoradi & Nemiroff (2015) model the joint population distributions of 1366 BATSE catalog LGRBs in the 5-dimensional LGRB property space of,

- (i) redshift (z),
- (ii) the intrinsic bolometric 1-second isotropic peak energy luminosity (L_{iso}) and its equivalent observable, the peak energy flux (P_{bol}).
- (iii) the intrinsic total isotropic bolometric emission (E_{iso}) and its equivalent observable, the bolometric fluence (S_{bol}).
- (iv) the intrinsic spectral peak energy (E_{pz}) and its equivalent observable, the observed spectral peak energy (E_{p}).
- (v) the intrinsic prompt gamma-ray duration as measured by the time interval during which 90% of the total gamma-ray energy of the LGRB is released (T_{90z}) and its equivalent observable, the observed duration (T_{90}).

while carefully taking into account the intrinsic correlations between the LGRB prompt gamma-ray properties and the detection threshold of BATSE Large Area Detectors (LADs).

To create our Monte Carlo universe of LGRBs, we use the inferred posterior distribution of the parameters of their

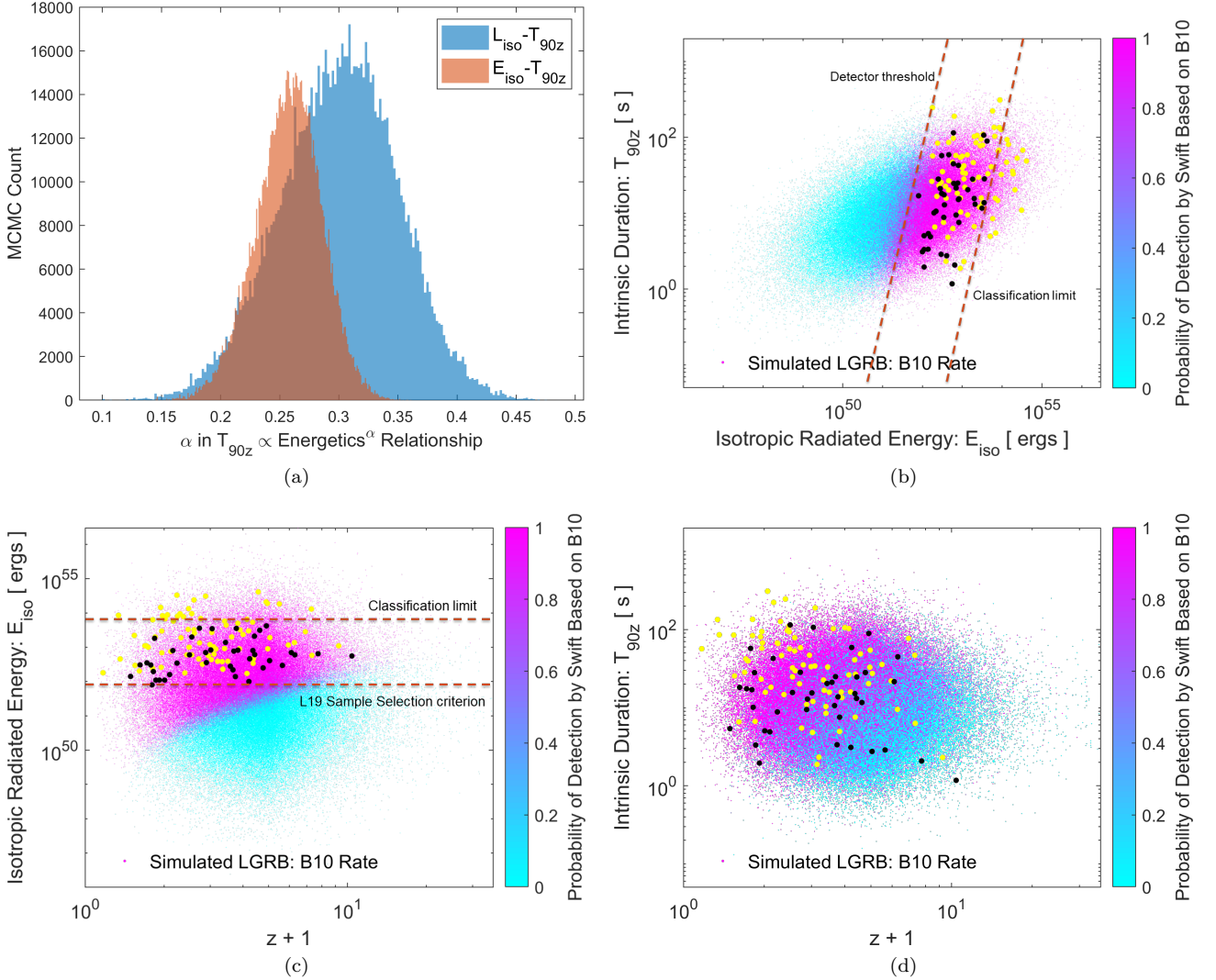


Figure 5. (a) The distribution of the exponent of $L_{\text{iso}} - T_{90z}$ and $E_{\text{iso}} - T_{90z}$ power-law relationships inferred from modeling the population distribution of 1336 BATSE LGRBs. (b) An illustration of the predicted underlying intrinsic distribution of LGRBs in the $E_{\text{iso}} - T_{90z}$ plane. Associated with each simulated LGRB is also a probability of it being detectable by the Swift BAT, represented by the cyan-magenta color-map. The overlaid yellow and black points represent the sample of bright radio-loud and radio-quiet LGRBs in L19 collected such that $E_{\text{iso}} \gtrsim 10^{52}$ [ergs]. The effective detection threshold of Swift BAT and the classification limit that separates the two classes of radio-loud and radio-quiet LGRBs are shown by the brown dashed lines. These two limits together potentially shape the narrow distribution of radio-quiet sample (black dots on this plane). (c) An illustration of the predicted underlying intrinsic distribution of LGRBs in the redshift ($z + 1$) – E_{iso} plane. The color codings of the plot objects are the same as those of plot (b). The two dashed lines represent the effective limits that are potentially shaping the distribution of radio-quiet sample of radio-quiet LGRBs in this plot. (d) An illustration of the predicted underlying intrinsic distribution of LGRBs in the ($z + 1$) – T_{90z} plane. The color codings of the plot objects are the same as those of plots (b) and (c).

multivariate model under the hypothesis of LGRBs following the LGRB rate density $\dot{\zeta}$ inferred by Butler et al. (2010),

$$\dot{\zeta}(z) \propto \begin{cases} (1+z)^{\gamma_0} & z < z_0 \\ (1+z)^{\gamma_1} & z_0 < z < z_1 \\ (1+z)^{\gamma_2} & z > z_1, \end{cases} \quad (1)$$

where the parameters, $(z_0, z_1, \gamma_0, \gamma_1, \gamma_2)$ for this equation are (0.97, 4.00, 3.14, 1.36, -2.92). The rate density estimate of Butler et al. (2010) is based on a careful multivariate modeling of Swift catalog of LGRBs. Previously we have used five other rate density models in Osborne et al. (2020a),

but found that the rate density estimate of B10 resulted in more accurate results than other models in predicting the redshifts of the BATSE catalog of LGRBs. Table 1 summarizes the inferred Pearson’s correlation coefficients between the four main prompt gamma-ray attributes of LGRBs considered in our LGRB world model. We refer the interested reader to Shahmoradi (2013c); Shahmoradi & Nemiroff (2015, 2019a); Shahmoradi & Nemiroff (2019b); Osborne et al. (2020a); Osborne et al. (2020b) for a comprehensive discussion of the modeling approach, and to Shahmoradi & Bagheri (2020); Shahmoradi et al. (2020); Kumbhare & Shahmoradi (2020) for details of the MCMC

sampling techniques used to construct the parameters posterior distribution.

Once we have a constrained parametric model for the joint distribution of the population distribution of LGRBs, we generate a Monte Carlo universe of LGRBs by randomly selecting a set of parameters for the LGRB world model from the posterior distribution of parameters and then generating a set of LGRB attributes (L_{iso} , E_{iso} , E_{pz} , T_{90z} , z) given the randomly-selected set of parameters for the LGRB world model.

Plot (a) of Figure 5 displays the distribution of the inferred exponent α for the power-law relationship between the intrinsic duration (T_{90z}) and energetics of LGRBs as measured by L_{iso} and E_{iso} . A realization of the $E_{\text{iso}} - T_{90z}$ relation is also displayed in plot (b) of Figure 5.

3.1 The $E_{\text{iso}} - T_{90z}$ correlation in radio-loud and radio-quiet LGRBs

Similar to L19, we confirm the existence of a weaker $E_{\text{iso}} - T_{90z}$ relationship in the population of radio-loud LGRBs ($\rho \sim 0.23 \pm 0.11$) compared to the radio-quiet sample of LGRBs ($\rho \sim 0.45 \pm 0.12$). However, bootstrapping results as depicted in plot (g) of Figure 3 indicate that the difference in the correlation strengths between the two radio classes is insignificant. Indeed, there is 10% probability that the underlying $E_{\text{iso}} - T_{90z}$ correlation in the radio-loud sample could be stronger than the corresponding correlation in the radio-quiet sample.

We have already shown in the previous sections of this manuscript and in Shahmoradi (2013c); Shahmoradi & Nemiroff (2015, 2019a); Shahmoradi & Nemiroff (2019b); Osborne et al. (2020a); Osborne et al. (2020b) that there is likely a strong intrinsic $E_{\text{iso}} - T_{90z}$ correlation in both LGRB and SGRB classes. This prediction readily explains the existence of a positive $E_{\text{iso}} - T_{90z}$ correlation in both samples of radio-loud and radio-quiet LGRBs. The strengths of the observed correlations are, however, much weaker than the predictions of our LGRB world model because of the strong effects of sample-incompleteness on the radio loud and radio-quiet LGRB samples.

Furthermore, the slight increase in $E_{\text{iso}} - T_{90z}$ correlation strength in the radio-quiet sample relative to the radio-loud sample of LGRBs can be also potentially explained away in terms of the subtle effects of radio classification and sample-incompleteness on the two LGRB populations. These two artificial fuzzy cuts on the radio-quiet sample are schematically illustrated by the brown dashed lines in plot (b) of Figure 5. The E_{iso} distribution of radio-quiet LGRBs is likely more affected by the detection threshold of Swift because radio-quiet LGRBs are generally less energetic.

However, unlike the radio-loud sample, the radio-quiet LGRBs are also limited by an upper E_{iso} fuzzy threshold which is purely due to the classification of LGRBs into two classes of radio-loud and radio-quiet. If an LGRB is bright enough in gamma-ray, its radio-emission will also be

come bright enough to be detectable. Therefore, gamma-ray-bright LGRBs are automatically classified as radio-loud LGRBs. The two aforementioned artificial cuts on the radio-quiet sample create a narrow distribution of LGRBs in the $E_{\text{iso}} - T_{90z}$ which artificially increases the observed $E_{\text{iso}} - T_{90z}$ correlation strength of radio-quiet LGRBs compared to the radio-loud sample.

3.2 The $z - E_{\text{iso}}$ correlation in radio-loud and radio-quiet LGRBs

We confirm the existence of a weaker $z - E_{\text{iso}}$ correlation in the population of radio-loud LGRBs ($\rho \sim 0.08 \pm 0.12$) compared to the radio-quiet sample of LGRBs ($\rho \sim 0.33 \pm 0.13$). However, bootstrapping results as depicted in plot (h) of Figure 3 indicate that the difference in the correlation strengths between the two radio classes is insignificant. Indeed, there is 9% probability that the underlying $E_{\text{iso}} - T_{90z}$ correlation in the radio-loud sample could be stronger than the corresponding correlation in the radio-quiet sample.

Furthermore, we hypothesize that the slight increase in $z - E_{\text{iso}}$ correlation strength in the radio-quiet sample relative to the radio-loud sample of LGRBs can be also again potentially explained away in terms of the subtle effects of classification and sample-incompleteness on the two LGRB populations. These two artificial fuzzy cuts on the radio-quiet sample are schematically illustrated by the brown dashed lines in Plot (c) of Figure 5. The E_{iso} distribution of radio-quiet LGRBs is likely more affected by the detection threshold of Swift because radio-quiet LGRBs are generally less energetic.

3.3 The $z - T_{90z}$ correlation in radio-loud and radio-quiet LGRBs

Similar to L19, we confirm the existence of a stronger $(z + 1) - T_{90z}$ anti-correlation in the population of radio-loud LGRBs ($\rho \sim -0.35 \pm 0.10$) compared to the radio-quiet sample of LGRBs ($\rho \sim -0.07 \pm 0.18$). However, bootstrapping results as depicted in plot (i) of Figure 3 indicate that the difference in the correlation strengths between the two radio classes is insignificant. Indeed, there is 9% probability that the underlying $z - T_{90z}$ correlation in the radio-loud sample could be weaker than the corresponding correlation in the radio-quiet sample.

Furthermore, the slight increase in $(z + 1) - T_{90z}$ anti-correlation strength in the radio-loud sample relative to the radio-quiet sample of LGRBs can be also potentially explained away in terms of the subtle effects of classification and sample-incompleteness on the two LGRB populations combined with the effects of the correlation strengths of $E_{\text{iso}} - T_{90z}$ and $(z + 1) - E_{\text{iso}}$ relationships in the two LGRB radio classes.

To illustrate the effects of $E_{\text{iso}} - T_{90z}$ and $(z + 1) - E_{\text{iso}}$ correlations on the $(z + 1) - T_{90z}$ correlation, we generate Monte Carlo realizations of the radio-loud and radio quiet LGRB samples, similar to the two observational samples

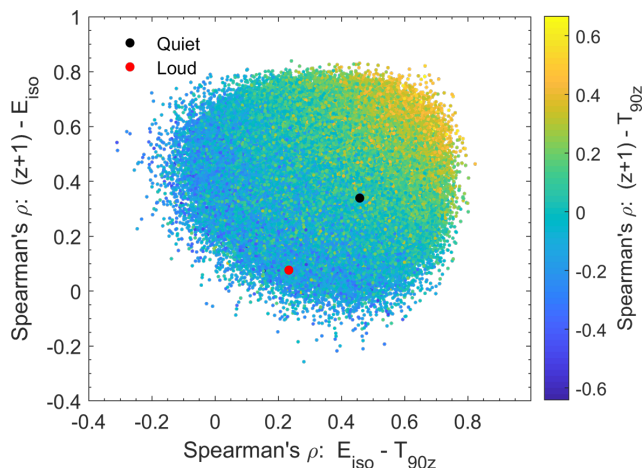


Figure 6. An illustration of the Monte Carlo simulations of the correlation coefficient strengths between the three LGRB intrinsic properties: redshift (represented by $z + 1$), E_{iso} , and T_{90z} . Each point on this plot represents a simulated LGRB sample of comparable size to the radio-loud and radio-quiet sample sizes of L19. The two overlaid black and red dots represent respectively, the locations of the radio-loud and radio-quiet samples of L19 on this plot, with the observed correlation coefficients of -0.36 and -0.08 for the $(z + 1) - T_{90z}$ relationship in the radio-loud and radio-quiet samples, respectively. The observed gradient of correlation strength in this plot is consistent with the observed $(z + 1) - T_{90z}$ correlation strengths for the two radio classes.

of L19. We do so by generating two samples that have the same distributions of redshift and E_{iso} as those of the observational radio-loud and radio-quiet samples, while fixing their $E_{\text{iso}} - T_{90z}$ and $(z + 1) - E_{\text{iso}}$ correlation strengths to their corresponding values in the observational samples. We then leave the T_{90z} distribution of the two synthetic samples to be randomly determined by our Monte Carlo simulations.

The above simulation scheme allows us to isolate the effects of $E_{\text{iso}} - T_{90z}$ and $(z + 1) - E_{\text{iso}}$ correlation strengths on the strength of the $z - T_{90z}$ correlation. The results of the Monte Carlo simulations are summarized in Table 2. As shown in the last column of the table, although the average simulated correlation strength of the $(z + 1) - T_{90z}$ relationship for the sample of radio-loud LGRBs does not fully match the corresponding observed value, the simulations indicate that a similar trend in correlation strengths with comparable differences to those of the observational samples can be reproduced purely based on the correlation strengths of $E_{\text{iso}} - T_{90z}$ and $(z + 1) - E_{\text{iso}}$ relationships. All of these Monte Carlo simulation results have been obtained without any a priori assumptions on the type of LGRBs, whether radio-loud or radio-quiet.

In other words, the observed $(z + 1) - T_{90z}$ correlation strength difference between the two radio-loud and radio-quiet samples likely has no physical origins but can be largely attributed to a complex combination of multiple sample incompleteness and selection effects in gamma-ray and radio detection, data collection, and redshift measurement.

To better illustrate the the above argument, we depict

in Figure 6 the distribution of the correlation coefficients between $(z + 1)$, E_{iso} , and T_{90z} for all Monte Carlo samples that have simulated. Overlaid on this distribution is the two observed radio-loud and radio-quiet samples of L19. From this figure, it is evident that a gradient in the strength of $(z + 1) - T_{90z}$ correlation exists as a function of the strengths of the $(z + 1) - E_{\text{iso}}$ and $E_{\text{iso}} - T_{90z}$ correlations. We note that this gradient purely results from the intrinsic gamma-ray properties of LGRBs inferred from our LGRB world model. We have made no assumptions on the existence of radio-loud or radio-quiet LGRBs in the aforementioned Monte Carlo simulations.

4 DISCUSSION

The existence of two classes of radio-loud and radio-quiet LGRBs with potentially different progenitors has been recently argued in the literature (e.g., Lloyd-Ronning & Fryer 2017; Lloyd-Ronning et al. 2019). Radio-loud LGRBs have been shown to be on average more energetic, longer-duration and exhibit weaker positive $E_{\text{iso}} - T_{90z}$ but stronger negative $(z + 1) - T_{90z}$ correlations than the radio-quiet class of LGRBs (Figure 3).

In this work, we have shown that much of the evidence in favor of such radio classification of LGRBs and their distinct progenitors can be purely attributed to the complex effects of detection thresholds of gamma-ray detectors (Shahmoradi & Nemiroff 2009, 2011) and radio telescopes (Chandra & Frail 2012) on the observed sample of bright LGRBs. Our arguments are built upon the recent discovery of a significant positive $E_{\text{iso}} - T_{90z}$ correlation ($\rho \sim 0.5 - 0.6$) in both populations of LGRBs and SGRBs by Shahmoradi (2013c); Shahmoradi & Nemiroff (2015). We have shown that the intrinsic $E_{\text{iso}} - T_{90z}$ correlation (Figure 5b) along with a potential positive correlation between the gamma-ray and radio luminosity of LGRBs (Figure 4) are sufficient conditions to generate much of the differing characteristics of radio-loud and radio-quiet LGRBs, without recourse to any radio classification of LGRBs.

Bootstrapping simulations indicate that some of the proposed spectral and temporal differences between the two proposed radio classes are not statistically significant (3). Furthermore, Monte Carlo simulations of the gamma-ray properties of the two radio classes reveal that more than 50% of the reported difference between the $(z + 1) - T_{90z}$ correlation strengths of the proposed radio classes can be readily and purely explained in terms of selection effects, sample incompleteness and the strong positive $E_{\text{iso}} - T_{90z}$ correlation in LGRBs.

In the light of the above arguments, it would seem likely that the presence of the very high energy GeV extended emission in the class of radio-loud LGRBs also results from the overall brighter light-curves of such LGRBs across all energy wavelengths, from radio to GeV.

The question of whether the radio telescopes have been sensitive enough to detect the faint LGRB radio emissions

Table 2. Correlations from L19 and from figure 6.

work used for correlations	$E_{\text{iso}} - T_{90z}$ correlation	$(z + 1) - E_{\text{iso}}$ correlation	$(z + 1) - T_{90z}$ correlation
L19 Radio loud GRBs	0.23	0.08	-0.36
L19 Radio quiet GRBs	0.46	0.40	-0.08
This work (correlation around red point)	0.23	0.08	-0.11
This work (correlation around black point)	0.46	0.40	0.05

has been raised previously (e.g., Chandra & Frail 2012; Resmi 2017). Given the proximity of the 3σ radio non-detection limits to the observed sample (Figure 1), it is conceivable that future radio telescopes with increased sensitivities will be able to detect the radio afterglows of more LGRB events (Chandra 2016). The numerical simulations of Burlon et al. (2015) also appear to support this conclusion. The future projects such as the Square Kilometer Array (Carilli & Rawlings 2004; Johnston et al. 2008) (whose operation is expected in 2027) and the recent upgrades to the existing telescopes such as the Giant Metrewave Radio Telescope (Swarup 1991; Ananthkrishnan 1995; Gupta 2014) and many others (e.g., Gupta et al. 2017) will provide a definite answer to the problem of radio-classification of LGRBs.

ACKNOWLEDGEMENTS

We thank Nicole Lloyd-Ronning at The University of New Mexico and Poonam Chandra at Tata Institute of Fundamental Research for kindly making their observational GRB data available to us. This work would have not been accomplished without the vast time and effort spent by many scientists and engineers who designed, built and launched the gamma-ray and radio observatories and were involved in the collection and analysis of GRB data.

REFERENCES

Ananthkrishnan S., 1995, *Journal of Astrophysics and Astronomy Supplement*, 16, 427
 Burlon D., Ghirlanda G., van der Horst A., Murphy T., Wijers R., Gaensler B., Ghisellini G., Prandoni I., 2015, arXiv preprint arXiv:1501.04629
 Butler N. R., Bloom J. S., Poznanski D., 2010, *The Astrophysical Journal*, 711, 495
 Carilli C., Rawlings S., 2004, arXiv preprint astro-ph/0409274
 Cenko S., et al., 2010, *The Astrophysical Journal*, 711, 641
 Chandra P., 2016, *Advances in Astronomy*, 2016
 Chandra P., Frail D. A., 2012, *The Astrophysical Journal*, 746, 156
 Dainotti M., Del Vecchio R., 2017, *New Astronomy Reviews*, 77, 23
 Efron B., Tibshirani R. J., 1994, *An introduction to the bootstrap*. CRC press
 Frail D. A., 2005, in *International Astronomical Union Colloquium*. pp 451–458

Frail D., Kulkarni S. R., Nicastro L., Feroci M., Taylor G., 1997, *Nature*, 389, 261
 Frail D. A., et al., 2001, *The Astrophysical Journal Letters*, 562, L55
 Fynbo J., et al., 2001, *Astronomy & Astrophysics*, 369, 373
 Groot P. J., et al., 1998, *The Astrophysical Journal Letters*, 493, L27
 Gupta Y., 2014, *The Metrewavelength Sky*, pp 197–202
 Gupta Y., et al., 2017, *Curr. Sci*, 113, 707
 Hancock P. J., Gaensler B. M., Murphy T., 2013, *The Astrophysical Journal*, 776, 106
 Heng K., Lazzati D., Perna R., Garnavich P., Noriega-Crespo A., Bersier D., Matheson T., Pahre M., 2008, *The Astrophysical Journal*, 681, 1116
 Hopkins A. M., Beacom J. F., 2006, *The Astrophysical Journal*, 651, 142
 Johnston S., et al., 2008, *Experimental astronomy*, 22, 151
 Kumar P., Zhang B., 2015, *Physics Reports*, 561, 1
 Kumbhare S., Shahmoradi A., 2020, arXiv e-prints, p. arXiv:2010.04190
 Lloyd-Ronning N. M., Fryer C. L., 2017, *Monthly Notices of the Royal Astronomical Society*, 467, 3413
 Lloyd-Ronning N. M., Gompertz B., Pe’er A., Dainotti M., Fruchter A., 2019, *The Astrophysical Journal*, 871, 118
 Margutti R., et al., 2013, *Monthly Notices of the Royal Astronomical Society*, 428, 729
 Meszaros P., 2002, *Annual Review of Astronomy and Astrophysics*, 40, 137
 Metzger M., Djorgovski S., Kulkarni S., Steidel C., Adelberger K., Frail D., Costa E., Frontera F., 1997, *Nature*, 387, 878
 Osborne J. A., Shahmoradi A., Nemiroff R. J., 2020a, *A Multilevel Empirical Bayesian Approach to Estimating the Unknown Redshifts of 1366 BATSE Catalog Long-Duration Gamma-Ray Bursts* (arXiv:2006.01157)
 Osborne J. A., Shahmoradi A., Nemiroff R. J., 2020b, arXiv e-prints, p. arXiv:2006.01157
 Piran T., 1999, *Physics Reports*, 314, 575
 Resmi L., 2017, *Journal of Astrophysics and Astronomy*, 38, 56
 Ricker G., et al., 2003, in *AIP Conference Proceedings*. pp 3–16
 Shahmoradi A., 2013a, arXiv preprint arXiv:1308.1097
 Shahmoradi A., 2013b, arXiv e-prints, p. arXiv:1308.1097
 Shahmoradi A., 2013c, *The Astrophysical Journal*, 766, 111
 Shahmoradi A., Bagheri F., 2020, arXiv e-prints, p. arXiv:2009.14229
 Shahmoradi A., Nemiroff R., 2009, in *AIP Conference Proceedings*. pp 425–427
 Shahmoradi A., Nemiroff R., 2011, *Monthly Notices of the Royal Astronomical Society*, 411, 1843
 Shahmoradi A., Nemiroff R. J., 2015, *Monthly Notices of the Royal Astronomical Society*, 451, 126
 Shahmoradi A., Nemiroff R. J., 2019a, arXiv preprint arXiv:1903.06989
 Shahmoradi A., Nemiroff R. J., 2019b, arXiv e-prints, p. arXiv:1903.06989

- Shahmoradi A., Bagheri F., Osborne J. A. e., 2020, arXiv e-prints, [p. arXiv:2010.00724](https://arxiv.org/abs/2010.00724)
- Swarup G., 1991, in International Astronomical Union Colloquium. pp 376–380
- Tu Z., Wang F., 2018, The Astrophysical Journal Letters, 869, L23
- Van Paradijs J., et al., 1997, Nature, 386, 686
- Woosley S., Bloom J., 2006, Annu. Rev. Astron. Astrophys., 44, 507